Tunable Swelling Kinetics in Core−Shell Hydrogel Nanoparticles

Daoji Gan and L. Andrew Lyon*

Contribution from the School of Chemistry and Biochemistry, Georgia Institute of Technology, Atlanta, Georgia 30332-0400

Received March 6, 2001

Abstract: Thermoresponsive, core−shell poly-*N*-isopropylacrylamide (p-NIPAm) nanoparticles (microgels) have been synthesized by seed and feed precipitation polymerization, and the influence of chemical differentiation between the core and shell polymers on the phase transition kinetics and thermodynamics has been examined. The results suggest that the core−shell architecture is a powerful one for the design of colloidal "smart gels" with tunable properties. To examine these materials, differential scanning calorimetry (DSC), ^{1}H NMR, and temperature-programmed photon correlation spectroscopy (TP-PCS) have been employed. These measurements show that the addition of small concentrations of a hydrophobic monomer (butyl methacrylate, BMA) into the particle shell produces large decreases in the rate of thermo-induced particle collapse. Conversely, these low levels of hydrophobic modification do not perturb the thermodynamics of the particle phase transition. When these results are examined in light of previous studies of macroscopic hydrogels, they suggest that the formation of a thin, stable skin layer at the particle exterior during the early stages of particle collapse is the rate limiting factor in particle deswelling. Finally, the hydrophobicity (BMA content) of the shell determines the magnitude of the hydrogel collapse rate, while the thickness of the BMA containing region does not impact the observed kinetics. Together, these results suggest that control over the kinetics of microgel deswelling events can be accomplished simply by modification of the particle periphery, and therefore do not require homogeneous modification of the entire polymer structure.

Introduction

The design of submicron-sized, core−shell hydrogel particles that undergo sharp, reversible, kinetically tunable volume phase transitions in response to temperature is reported. The hydrogel is largely composed of a thermoresponsive polymer (poly-*N*-isopropylacrylamide, p-NIPAm) that is known to undergo a reversible, temperature-induced coil−globule transition or phase separation.[1,2] We have shown previously that synthesis of this hydrogel as submicron-sized particles yields a colloidal material whose deswelling thermodynamics can be tuned by chemical manipulation of a thin shell of a dissimilar hydrogel applied to the core particle.[3] In this contribution, we use a similar methodology to demonstrate that small chemical modifications made to the particle exterior are sufficient to produce large magnitude changes in the particle deswelling kinetics, without modulation of the deswelling energetics. In this fashion, the temperature and the rate of hydrogel collapse can be decoupled and therefore tuned independently of one another.

The historical and continued interest in environmentally responsive polymers can be traced to their potential applications in numerous fields, including drug delivery,[4−6] chemical separations,[7−12] sensors,[13] biomaterials,[14,15] cell culture systems,[16−19] and catalysis.[20,21] Temperature responsive polyalkylacrylamides, specifically poly-*N*-isopropylacrylamide,[2] have been the most heavily studied of these polymers, as they represent a convenient and well-behaved model system for the construction of numerous "environmentally switchable" soft materials.[22−24] Because of the versatility and unique behavior of these polymers, there has been a growing interest into

* To whom correspondence should be addressed: (e-mail) lyon@chemistry.gatech.edu.

(1) Pelton, R. *Adv. Colloid. Interface Sci.* **2000**, *85*, 1−33.
(2) Shibayama, M.; Tanaka, T. *Volume Phase Transition and Related Phenomena of Polymer Gels*; Springer-Verlag: Berlin, 1993; Vol. 109, pp 1−62.
(3) Jones, C. D.; Lyon, L. A. *Macromolecules* **2000**, *33*, 8301−8306.
(4) Jeong, B.; Bae, Y. H.; Lee, D. S.; Kim, S. W. *Nature* **1997**, *388*, 860−862.
(5) Hoffman, A. *"Intelligent" Polymers*; Park, K., Ed.; American Chemical Society: Washington, D.C., 1997; pp 485−498.
(6) Brondsted, H.; Kopecek, J. *Pharm. Res.* **1992**, *9*, 1540−1545.
(7) Kayaman, N.; Kazan, D.; Erarslan, A.; Okay, O.; Baysal, B. M. *J. Appl. Polym. Sci.* **1998**, *67*, 805−814.
(8) Kawaguchi, H.; Fujimoto, K. *Bioseparation* **1998**, *7*, 253−258.
(9) Liang, D.; Song, L.; Zhou, S.; Zaitsev, V. S.; Chu, B. *Electrophoresis* **1999**, *20*, 2856−2863.
(10) Liang, D.; Zhou, S.; Song, L.; Zaitsev, V. S.; Chu, B. *Macromolecules* **1999**, *32*, 6326−6332.
(11) Buchholz, B. A.; Doherty, E. A. S.; Albarghouthi, M. N.; Bogdan, F. M.; Zahn, J. M.; Barron, A. E. *Anal. Chem.* **2001**, *73*, 157−164.
(12) Albargheuthi, M. N.; Barron, A. E. *Electrophoresis* **2000**, *21*, 4096−4111.
(13) Hu, Z. B.; Chen, Y. Y.; Wang, C. J.; Zheng, Y. D.; Li, Y. *Nature* **1998**, *393*, 149−152.
(14) Chen, G. P.; Ito, Y.; Imanishi, Y. *Biotechnol. Bioeng.* **1997**, *53*, 339−344.
(15) Shiroya, T.; Yasui, M.; Fujimoto, K.; Kawaguchi, H. *Colloids Surf., B* **1995**, *4*, 275−285.
(16) Bohanon, T.; Elender, G.; Knoll, W.; Koeberle, P.; Lee, J.-S.; Offenhaeusser, A.; Ringsdorf, H.; Sackmann, E.; Simon, J.; et al. *J. Biomater. Sci., Polym. Ed.* **1996**, *8*, 19−39.
(17) Kwon, O. H.; Kikuchi, A.; Yamato, M.; Sakurai, Y.; Okano, T. *J. Biomed. Mater. Res.* **2000**, *50*, 82−89.
(18) Yamato, M.; Kwon, O. H.; Hirose, M.; Kikuchi, A.; Okano, T. *J. Biomed. Mater. Res.* **2000**, *55*, 137−140.
(19) Ista, L. K.; Perez-Luna, V. H.; Lopez, G. P. *Appl. Environ. Microbiol.* **1999**, *65*, 1603−1609.
(20) Bergbreiter, D. E.; Case, B. L.; Liu, Y.-S.; Caraway, J. W. *Macromolecules* **1998**, *31*, 6053−6062.
(21) Chen, C. W.; Akashi, M. *Polym. Adv. Technol.* **1999**, *10*, 127−133.
(22) Irie, M. *Stimuli-Responsive Poly(N-isopropylacrylamide). Photo- and Chemical-Induced Phase Transitions*; Springer-Verlag: Berlin, 1993; Vol. 110, pp 49−65.

10.1021/ja010609f CCC: $20.00
Published on Web 07/12/2001

Table 1. Chemical Compositions and Radii of p-NIPAm Core−Shell Hydrogel Particles

	molar ratio of core (to NIPAm %)				molar ratio of shell (to NIPAm %)			
	BIS	BMA		R_{core}	BIS	BMA		$R_{core-shell}$
sample	(in feed)	feed	obsd[a]	(nm)[b]	(in feed)	feed	obsd[a]	(nm)[b]
A	5.0	0		138				
B	5.0	0		138	5.0	0		192
C	5.0	0		142	5.0	1.0	0.95	188
D	5.0	1.0	0.92	137	5.0	1.0	0.89	195
E	5.0	0		145	5.0	2.0	1.90	187
F1	5.0	0		135	5.0	1.0	0.94	205
F2	5.0	0		135	5.0	1.0	0.92	180
F3	5.0	0		135	5.0	1.0	0.96	173
F4	5.0	0		135	5.0	1.0	0.93	155
F5	5.0	0		135	5.0	0		214
G0	5.0	0		147	5.0	0		206
G1	5.0	0		147	5.0	0.5	0.46	210
G2	5.0	0		147	5.0	1.0	0.94	194
G3	5.0	0		147	5.0	1.5	1.40	193
G4	5.0	0		147	5.0	2.0	1.87	197
G5	5.0	0		147	5.0	2.5	2.43	196

[a] Observed by ^{1}H NMR in $CDCl_3$. [b] Mean particle radii measured by PCS at 25 °C.

responsive latices that possess a more advanced architecture. Along these lines, core−shell or core−corona particles have been synthesized either to introduce spatially localized chemical functionalities to the particle,[25] to impart thermoresponsivity to nonresponsive particles, [26] or to modify a specific physical property of the latex.[27,28] We have shown that this approach can generate multiresponsive hydrogels that are value-added; the particles have physicochemical properties that do not arise from a simple summation of the two hydrogel behaviors.[3] The unusual behavior brought about by the core−shell morphology results from the important role played by the hydrogel particle periphery in the volume phase transition. Since the particle exterior is typically involved in the initial stages of microgel deswelling,[29,30] the chemical details of the particle shell should have a strong influence over the further collapse of the particle. In other words, the core−shell hydrogel system is one wherein the shell polymer has a chemical and/or mechanical influence over the solvation of the core component. In this paper, we exploit this effect to create an architecture wherein the interactions between the core and shell polymers *do not* perturb the thermodynamics of the phase transition, but instead conspire to produce large changes in the *kinetics* of the phase transition.

Experimental Section

Materials. *N*-Isopropylacrylamide (NIPAm) was obtained from Aldrich and recrystallized from hexane (J. T. Baker) before use. Both butyl methacrylate (BMA) and *N*,*N*-dimethylformamide (DMF) (Aldrich) were distilled under reduced pressure. *N*,*N*′-Methylenebis(acrylamide) (BIS), sodium dodecyl sulfate (SDS), and ammonium persulfate (APS) were used as received from Aldrich. Water used in all syntheses and measurements was distilled and then purified using a Barnstead E-Pure system operating at a resistance of 18 MΩ. A 0.2 μm filter incorporated into this system removed particulate matter.

Polymerization. A detailed procedure for the preparation of core−shell hydrogel particles by two-stage (seed and feed), free radical precipitation polymerization is described elsewhere.[3] Core particles were synthesized from various ratios of NIPAm (monomer, 1.13 g, 10 mmol, 1 equiv); BMA (comonomer, either 0.0 or 0.01 equiv) predissolved in DMF at a concentration of 5 mg/mL, BIS (cross-linker, 0.05 equiv), and SDS (surfactant, 0.01 equiv) in 150 mL of nitrogen-purged water. The reaction mixture was kept at 70 °C under a stream of nitrogen for 2 h. Following the addition of APS (initiator, 0.01 equiv), the polymerization was carried out at 70 °C for 6 h under a nitrogen atmosphere. This first batch of hydrogel particles (core) served as nuclei in a second stage of polymerization (shell addition). Prior to shell addition, the core was purified by dialysis (Spectra/Por 7 dialysis membrane, MWCO 10 000, VWR) first against water/DMF (volume ratio: 80/20) for 7 days and then against pure water for an additional 14 days. In the shell synthesis, a solution of the desired core particles (75 mL) was heated to 70 °C, whereupon a feed of NIPAm (varying from 0.395 to 0.565 g depending on the desired shell thickness, 1 equiv), BMA (varying from 0.00 to 0.025 equiv), BIS (0.05 equiv), SDS (varying from 0.005 to 0.02 equiv), and 75 mL of degassed water was introduced to the reaction flask. This solution was kept at 70 °C under a stream of nitrogen for 2 h. Polymerization was then initiated by the addition of APS (0.01 equiv); polymerization was again carried out for 6 h. All core−shell particles were then purified via dialysis using the same 21-day procedure described above. It should be noted that under these synthesis conditions, the core particles are deswollen polymer globules, while the monomers are largely soluble in the continuous phase. It is therefore expected that the degree of core swelling by monomer is very minimal, thereby resulting in a low degree of interpenetration of the core and shell during shell addition. Furthermore, the relatively high level of cross-linking (5 mol %) will tend to limit the degree of interpenetration when the particles cool and reswell. Indeed, we have previously observed discrete core−shell structure by transmission electron microscopy of differentially stained hydrogels prepared in a nearly identical fashion. Such analysis is not readily attainable in this case, however, due to the lack of any significant spatially heterogeneous chemistry in these gels.

To minimize the effects of variable core sizes on the thermodynamic and kinetic measurements, within each particle series (F1−F5 and G0−G5) the same batch of core particles was used to construct the core−shell particles. This is reflected by the consistent core sizes within each series, as shown in Table 1. The approximate particle sizes were controlled via varying the concentration of SDS during polymerization. In general, higher concentrations of SDS result in smaller particle sizes,

(23) Gehrke, S. H. *Synthesis, Equilibrium Swelling, Kinetics, Permeability and Applications of Environmentally Responsive Gels*; Springer-Verlag: Berlin, 1993; Vol. 110, pp 82−144.
(24) Kim, J.-C.; Bae, S. K.; Kim, J.-D. *J. Biochem. (Tokyo)* **1997**, *121*, 15−19.
(25) Duracher, D.; Sauzedde, F.; Elaissari, A.; Perrin, A.; Pichot, C. *Colloid Polym. Sci.* **1998**, *276*, 219−231.
(26) Matsuoka, H.; Fujimoto, K.; Kawaguchi, H. *Polym. J.* **1999**, *31*, 1139−1144.
(27) Hazot, P.; Delair, T.; Elaissari, A.; Pichot, C.; Chapel, J. P.; Davenas, J. *Macromol. Symp.* **2000**, *150*, 291−296.
(28) Senff, H.; Richtering, W.; Norhausen, C.; Weiss, A.; Ballauff, M. *Langmuir* **1999**, *15*, 102−106.
(29) Wu, C.; Zhou, S. *Macromolecules* **1997**, *30*, 574−576.
(30) Wu, C. *Polymer* **1998**, *39*, 4609−4619.

as predicted by homogeneous nucleation theory.[31,32] The chemical compositions and mean equilibrium swelling radii of the hydrogel particles are listed in Table 1.

^{1}H NMR. The incorporation rate of BMA in these syntheses was determined by a NMR method reported elsewhere.[33] ^{1}H NMR spectra of the polymers were recorded in $CDCl_3$ solutions with the solvent proton signal as a reference, using a Varian Unity 500 MHz spectrometer.

Photon Correlation Spectroscopy. Temperature-programmed photon correlation spectroscopy (TP-PCS, Protein Solutions, Inc.) was used to determine the mean particle sizes and particle size distributions, as described previously.[3,34] This technique has been applied extensively to the characterization of such materials, as it allows for in situ size characterization of soft materials that cannot be reliably sized by electron microscopies due to deformation and/or dehydration under vacuum.[25,29,30,35−40] The dispersed particles in water were allowed to equilibrate thermally for 10 min before measurements were taken at each temperature. In the data presented below, each data point at a given temperature represents the average value of 20 measurements, with a 20 s integration time for each measurement. Hydrodynamic radii of the particles were calculated from diffusion coefficients using the Stokes−Einstein equation. All correlogram analyses were performed using manufacturer-supplied software (Dynamics v.5.25.44, Protein Solutions, Inc.).

Differential Scanning Calorimetry (DSC). Nonequilibrium DSC measurements were carried out using a Perkin-Elmer DSC-7. Baselines were collected at a heating rate of 2.5 °C/min over the temperature range of 20−60 °C, using 60 μL of water in both reference and sample cells.[41] DSC measurements were taken at a heating rate of 2.5 °C/min from 20 to 60 °C, with 60 μL of a polymer/water solution (30 mg/mL) in the sample cell. The transition temperature was determined from the intersection point of the baseline and the tangent of the endothermic curve.[42,43] If the polymer sample thermally equilibrates at a rate that is slower than the temperature scan (nonequilibrium measurement), a lag in the heat flow is observed.[44] As these measurements are performed in this nonequilibrium mode at a constant heating rate, the width of the peak is inversely proportional to the rate at which the sample attains thermal equilibrium. Hence, broadening of the DSC peak indicates a slower rate of particle deswelling.[44−46] As indicated in the text, the width of the transition peak was normalized for variability in particle size as follows:

$$\text{peak width (norm)} = \text{peak width (measured)}/r^2\ (^\circ\text{C/nm}^2) \quad (1)$$

where r is the particle radius determined by TP-PCS at 25 °C. This inverse power-law dependence of collapse rate on particle radius is well established, with the theoretical exponent being 2.[47,48] The enthalpy change was normalized to kJ/mol NIPAm according to the compositions of the hydrogel particles. These thermodynamic and kinetic data are listed in Table 2.

Table 2. Thermodynamic and Kinetic Data Obtained from DSC Measurements of Core−Shell Microgel Solutions[a]

sample	ΔH (kJ/mol NIPAm)	peak width (°C)	peak width/r^2 (°C/nm^2, $\times 10^{-4}$)
B	4.34 ± 0.06	3.9 ± 0.1	1.06 ± 0.03
C	4.37 ± 0.07	8.5 ± 0.1	2.40 ± 0.04
D	4.32 ± 0.09	9.0 ± 0.1	2.37 ± 0.03
E	4.35 ± 0.09	10.8 ± 0.2	3.09 ± 0.05
F1	4.30 ± 0.15	12.1 ± 0.2	2.88 ± 0.05
F2	4.33 ± 0.20	9.1 ± 0.1	2.81 ± 0.04
F3	4.36 ± 0.16	7.2 ± 0.1	2.41 ± 0.04
F4	4.34 ± 0.16	6.3 ± 0.1	2.62 ± 0.05
F5	4.29 ± 0.17	4.1 ± 0.1	0.90 ± 0.02
G0	4.35 ± 0.17	4.3 ± 0.1	1.01 ± 0.02
G1	4.34 ± 0.25	7.7 ± 0.1	1.75 ± 0.03
G2	4.30 ± 0.13	10.6 ± 0.2	2.82 ± 0.06
G3	4.33 ± 0.15	11.3 ± 0.2	3.03 ± 0.05
G4	4.37 ± 0.19	12.7 ± 0.1	3.27 ± 0.03
G5	4.31 ± 0.20	14.4 ± 0.2	3.75 ± 0.05

[a] Average of five measurements.

Results

The syntheses and resultant properties of the particles prepared for these studies are summarized in Table 1. Samples A−E are various "control" particles, while series F and G have variable shell thicknesses and shell BMA concentrations, respectively. As described in the Experimental Section, core−shell hydrogel particles were prepared via two-stage, free radical precipitation polymerization, as described previously.[3] The dispersed p-NIPAm particle solution prepared in the first stage represents the particle core, where subsequent polymerization leads to formation of the particle shell. It has been demonstrated that the polymer formed in the second stage preferentially grows around the existing particles, which act as nuclei for further polymerization.[3] Due to the poor solubility of p-NIPAm in water above the lower critical solution temperature (LCST), the core particles collapse to a high density and thus hinder the penetration of the growing shell during the second stage of polymerization at 70 °C. Hindrance of core−shell interpenetration is further assisted by the good solubility of the shell monomers in the continuous phase. We have shown previously by TEM analysis that these conditions lead to core−shell particles that do not display large degrees of interpenetration. As evidence of the addition of polymer to the existing particles, core−shell microgels show significantly increased sizes in comparison with the core particles. The hydrodynamic radii reported in Table 1 were obtained by photon correlation spectroscopy (PCS) at 25 °C. Furthermore, the calculated polydispersity for all particles lies below 25% (20% is the typical polydispersity) and is largely independent of temperature (Supporting Information), indicating that polymer produced in the second polymerization stage is added to the core particles and does not nucleate a new particle population.

Hydrogel particles with low cross-linking densities can be dispersed in $CDCl_3$, thus their chemical compositions can be determined via ^{1}H NMR.[33] By comparing the peak area at 0.90 ppm (terminal methyl protons of butyl side chains) with the peak area at 4.01 ppm (methine proton from isopropyl groups), the molar ratio of BMA to NIPAm in the polymer was calculated

(31) McPhee, W.; Tam, K. C.; Pelton, R. *J. Colloid Interface Sci.* **1993**, *156*, 24−30.
(32) Wu, X.; Pelton, R. H.; Hamielec, A. E.; Woods, D. R.; McPhee, W. *Colloid Polym. Sci.* **1994**, *272*, 467−477.
(33) Kanazawa, H.; Kashiwase, Y.; Yamamoto, K.; Matsushima, Y.; Kikuchi, A.; Sakurai, Y.; Okano, T. *Anal. Chem.* **1997**, *69*, 823−830.
(34) Debord, J. D.; Lyon, L. A. *J. Phys. Chem. B* **2000**, *104*, 6327−6331.
(35) Saunders, B. R.; Vincent, B. *Adv. Colloid Interface Sci.* **1999**, *80*, 1−25.
(36) Duracher, D.; Elaissari, A.; Pichot, C. *Macromol. Symp.* **2000**, *150*, 305−311.
(37) Duracher, D.; Elaissari, A.; Pichot, C. *Colloid Polym. Sci.* **1999**, *277*, 905−913.
(38) Snowden, M. J.; Chowdhry, B. Z.; Vincent, B.; Morris, G. E. *J. Chem. Soc., Faraday Trans.* **1996**, *92*, 5013−5016.
(39) Yi, Y. D.; Oh, K. S.; Bae, Y. C. *Polymer* **1997**, *38*, 3471−3476.
(40) Yi, Y. D.; Bae, Y. C. *J. Appl. Polym. Sci.* **1998**, *67*, 2087−2092.
(41) Woodward, N. C.; Chowdhry, B. Z.; Leharne, S. A.; Snowden, M. J. *Eur. Polym. J.* **2000**, *36*, 1355−1364.
(42) Shibayama, M.; Suetoh, Y.; Nomura, S. *Macromolecules* **1996**, *29*, 6966−6968.
(43) Shibayama, M.; Mizutani, S.-Y.; Nomura, S. *Macromolecules* **1996**, *29*, 2019−2024.
(44) Otake, K.; Inomata, H.; Konno, M.; Saito, S. *Macromolecules* **1990**, *23*, 283−289.
(45) Zhang, X.-Z.; Zhuo, R.-X. *Langmuir* **2001**, *17*, 12−16.
(46) Kawasaki, H.; Sasaki, S.; Maeda, H. *Langmuir* **1998**, *14*, 773−776.
(47) Li, Y.; Tanaka, T. *J. Chem. Phys.* **1990**, *92*, 1365−1371.
(48) Matsuo, E. S.; Tanaka, T. *J. Chem. Phys.* **1988**, *89*, 1695−1703.

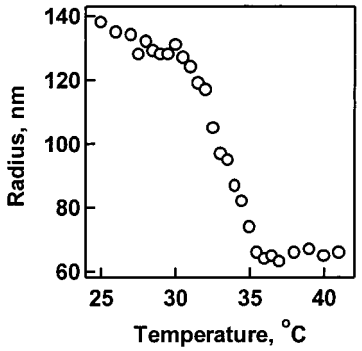

Figure 1. Hydrodynamic radius of sample A (p-NIPAm microgel) as a function of temperature measured by TP-PCS under equilibrium conditions in water.

(Table 1).[33] As expected, the incorporation rate of BMA is not 100%, yet the relative concentrations change monotonically with the monomer feed concentration, with the actual incorporation rate varying from 89% to 96%. PCS can also be performed in a temperature-programmed mode (TP-PCS) to measure the phase transition temperature of the microgels,[3,39,40] as shown in Figure 1 for sample A (p-NIPAm core). As is typical for cross-linked microgels, the curve has a finite breadth, with the transition occurring over about 5 degrees for these samples.[36,37] The magnitude of the phase transition is also related to the cross-linking density; a 10-fold volume decrease is observed for a typical p-NIPAm microgel with a 5% cross-linker density. The shape and position of these curves are corroborated by measurements of the scattered light intensity as a function of temperature (Supporting Information). Together, these results compare well with those reported by others for similarly prepared particles.[32,35−37,49]

As described above, the introduction of a shell to the particles should be accompanied by an increase in hydrodynamic radius at both low and high temperature. This effect is shown in Figure 2, which compares the LCST curve for samples A−C with respect to radius (panel a) and volume (panel b). Sample B is a p-NIPAm (core)/p-NIPAm (shell) particle, while sample C is a p-NIPAm (core)/p-NIPAm-*co*-BMA (shell) particle with 1 mol % of BMA incorporated into the shell. The swollen radii of both core−shell samples have increased by ∼50 nm, while the collapsed radii are ∼35 nm larger. All three curves also show the same transition breadth (∼5 degrees) with the core−shell volume change (∼8−9-fold) being slightly smaller than that of the parent core particle. It is interesting to note that the position of the LCST is also very similar for the three particles, despite the fact that sample C contains ∼1% BMA in the shell, whereas sample B contains no BMA. Together, these results demonstrate that small amounts of a "contaminant" monomer in the hydrogel shell do not strongly perturb the thermodynamics of hydrogel solvation. However, this should be true only for low concentrations of BMA, where the hydrophobic monomers are largely noninteracting and no significant phase separation is possible.

It is well-known that the enthalpy change (ΔH) resulting from water dissociation at the p-NIPAm LCST is large enough to be detected via conventional DSC.[43,44,46,50] The differential heat flow in microgel solutions can therefore be used as a measure of the magnitude, temperature, and (in nonequilibrium scans) the rate of particle collapse.[44−46] Figure 3a shows DSC thermograms for core−shell particles as a function of shell thickness (F1−F5), where samples F1−F4 contain a 1%

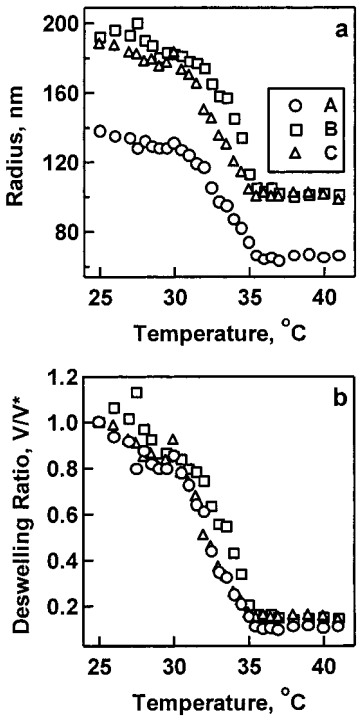

Figure 2. Hydrodynamic radii (panel a) and deswelling ratios (panel b) of samples A (p-NIPAm core), B (p-NIPAm core/p-NIPAm shell), and C (p-NIPAm core/p-NIPAm-*co*-BMA shell) as a function of temperature in water. The sizes and specific chemical compositions of the particles are listed in Table 1.

concentration of BMA (thicknesses shown in Table 1), and sample F5 contains only p-NIPAm homopolymer in the shell. To directly compare these scans, the volume and concentration of the polymer solutions used in each measurement were the same (60 μL of a 30 mg/mL solution). From these data, one finds that the initial transition temperature, which is defined as the intersection of the baseline and the tangent line of the endothermic peak,[43] is ∼32 °C for all five samples. The enthalpy change associated with the transition is calculated via integration of the endothermic peak. All samples show quite similar values, ∼4.33 kJ/mol NIPAm, which is in agreement with values reported in the literature.[44,46,50] The similarity of these ΔH values suggests similar levels of water dissociation from p-NIPAm in all samples. However, significant differences in the endothermic peak positions and widths do exist; these differences reflect a change in the *rate* of water dissociation from the microgel. As shown in Figure 3b, the width of the endotherm increases in a roughly monotonic fashion as the thickness of the BMA-containing shell is increased. In contrast, when a ∼80-nm thick shell of p-NIPAm is added without the introduction of BMA (sample F5) a peak that is narrower than all BMA-containing particles is obtained. While there is clearly a dependence on shell thickness, it should be noted that increases in absolute particle size accompany shell thickness increases since these samples are all built upon the same size core particles. To account for variations in particle size, the peak widths were normalized to the square of the particle radius via eq 1 (Figure 3c). This normalization procedure is derived from the well-known behavior of spherical macrogels, which swell at a rate that is inversely proportional to the radius squared.[47,48] Following normalization, all the samples having 1 mol % BMA in the shell show similar collapse rates, while F5 (no BMA) still undergoes a significantly faster deswelling event. The results of these and all other DSC measurements are listed in Table 2.

(49) Senff, H.; Richtering, W. *J. Chem. Phys.* **1999**, *111*, 1705−1711.
(50) Kawasaki, H.; Sasaki, S.; Maeda, H.; Nishinari, K. *Langmuir* **2000**, *16*, 3195−3199.

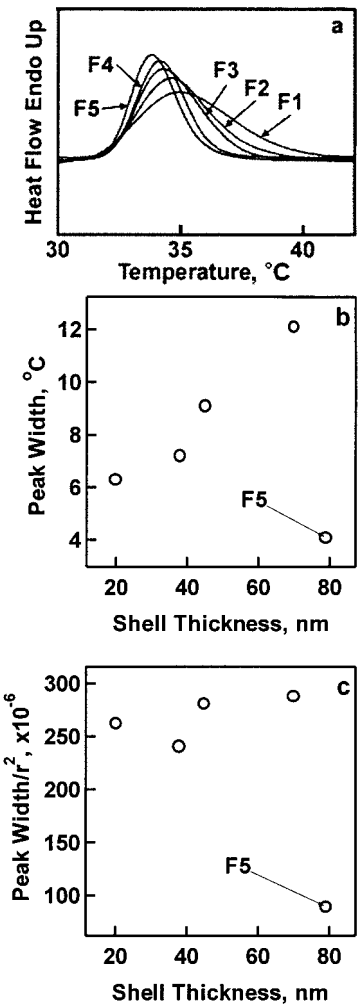

Figure 3. DSC measurements of sample series F1−F5 using 60 μL of 30 mg/mL polymer solution at a heating rate of 2.5 °C/min. Samples F1−F4 are p-NIPAm (core)/p-NIPAm-*co*-BMA (shell) (1 mol-% BMA) particles with different shell thickness (listed in Table 1), while F5 is the p-NIPAm (core)/p-NIPAm (shell) particle with ∼80 nm of shell thickness. Panel a shows the baseline-corrected DSC curves. The transition width is plotted as a function of shell thickness in panel b, showing a monotonic increase in peak width with shell thickness, as well as a large difference between the BMA containing particles (F1−F4) and the p-NIPAm homopolymer (F5). Panel c shows the peak width corrected for particle size as a function of shell thickness. Only small differences in the peak width are now evident for the BMA-modified particles, while F5 displays a faster deswelling rate. Standard deviations (five measurements) for these data are given in Table 2 and are roughly represented by the size of the data points.

To understand the influence of BMA localization on the particle collapse kinetics, two samples (D and E) were prepared to contain the same total BMA concentration (1 mol %). The synthesis conditions were such that sample E contains the entire BMA concentration in the shell (2% shell BMA concentration, 0% core BMA concentration), while both the core and the shell of sample D contain 1 mol % of BMA (see Table 1). Figure 4a shows the TP-PCS curves for both samples D and E. Again, the same LCST behavior is observed for the two samples, with the magnitude, position, and sharpness of the collapse being nearly identical for the two samples. However, when the kinetics of collapse are probed by DSC (Figure 4b), sample E shows a much broader endothermic peak than that observed for sample D. While the particle sizes in this case are not identical, the faster responding sample (Sample D) contains the larger particles. Normalizing for particle size effects will therefore only

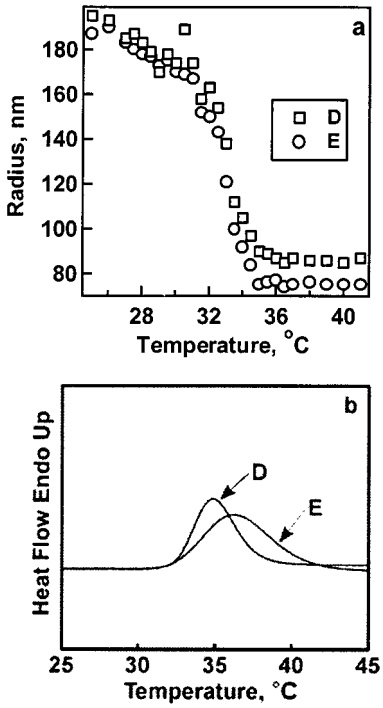

Figure 4. Hydrodynamic radii as a function of temperature measured by TP-PCS under equilibrium conditions in water (panel a) and DSC curves measured at a heating rate of 2.5 °C/min for samples D and E. Both the core and shell of sample D contain 1 mol % BMA, while sample E contains 2 mol % of BMA in the shell but with no BMA in the core. D and E have the same LCST behavior, but E shows a much broader (slower) transition in DSC measurements.

serve to increase the difference between the two particle collapse rates. It should also be noticed that sample D displays a very similar peak width to samples F1−F4 (see Table 2 and Supporting Information). To compare these particles with respect to shell thickness effects, we can essentially view sample D as having a BMA-containing shell thickness that is equal to the particle radius (infinitely thick shell). This similarity in collapse rates between samples D and F1−F4 further amplifies the conclusion that shell thickness plays little role in the determination of the deswelling kinetics.

The influence of BMA shell concentration on the collapse kinetics can be seen in the behavior of samples G0−G5 (Figure 5). To limit any phase-separation effects and to maintain the original phase transition behavior of p-NIPAm microgel, the BMA content in the shell was kept below 3 mol %. All the core−shell particles were prepared using the same batch of core solution to avoid any inaccuracy in the DSC measurements caused by variation of core size. As shown in Table 2, the normalized enthalpy change associated with the transition is nearly identical for these samples, which is consistent with the data presented above. Again, subtle changes in the BMA content do not significantly impact the overall thermodynamics of the particle phase transition. However, the width of the peak increases as the BMA content in the shell increases (Figure 5a). The radius-normalized peak width is observed to increase in a roughly linear fashion with BMA content, as shown in Figure 5b. From these results, it is evident that a mechanism is operative wherein small changes in the microgel hydrophobicity at the particle periphery result in significant modulation of the phase transition kinetics, without perturbing the energetics of the event. Our interpretation of these observations is presented in the following section.

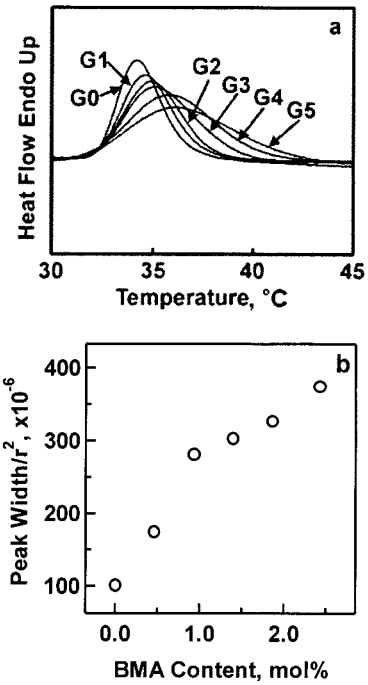

Figure 5. DSC curves (panel a) and their normalized DSC peak widths (Panel b) as a function of shell BMA content for sample series G0−G5. The normalized peak width increases monotonically with BMA content. Standard deviations (five measurements) for these data are given in Table 2 and are roughly represented by the size of the data points.

Discussion

The data in Figure 1 illustrate typical phase transition behavior of spherical microgels. P-NIPAm microgels, which are cross-linked latex particles usually prepared by free radical precipitation polymerization, differ from macrogels in a number of aspects. The microgel volume phase transition displays a finite width, and is generally regarded to be a continuous transition.[29,30] This is in contrast to the discontinuous, first-order phase transition often observed for macrogels.[2,48,51] While a number of potential sources for this deviation from first-order behavior exist, the most compelling evidence argues for heterogeneity in the microgel structure that does not exist in macrogels. Specifically, micron sized gels prepared by precipitation polymerization possess a polydispersity in the sub-chain length.[29,30] It has been proposed that as the temperature increases, the sub-network having a longer sub-chain undergoes a phase transition before the sub-network with a shorter chain.[29,30] Therefore, different parts of the gel network undergo a phase transition at different temperatures, leading to breadth in the measured curve. Others have found that the consumption of cross-linking monomers occurs much more quickly than that of NIPAm during precipitation polymerization, and therefore concluded that a radial gradient of cross-linking densities exists in microgels, with the cross-linker content decreasing from the center of particles toward the periphery.[31,32] The presence of this gradient has also been shown by ^{1}H NMR relaxation experiments.[52] As such, one might expect that microgel phase transitions would occur beginning at the microgel periphery and proceed toward the interior. In terms of the data in Figure 1, the points corresponding to small size decreases just past 30 °C should therefore correspond to the formation of a dehydrated shell of polymer surrounding a hydrated core. Further deswelling then occurs by a thickening of the dehydrated layer, and a concomitant decrease in the radius of the swollen core. The formation of a "skin layer" has been observed for macrogels prepared by bulk solution polymerization, where a thin layer of dense, collapsed polymer network forms on the gel surface following a temperature jump across the LCST.[45,48,53−56] However, in the case of macrogels, this is often an unstable state, as the positive osmotic pressure in the gel interior is sufficient to break down the skin layer and allow further expulsion of water from the material.[48,53] Conversely, this instability does not occur in microgels, where the skin layer contributes to a thermodynamically stable coexistence of collapsed and swollen phases, whcih in turn results in the curve broadening shown in Figure 1 (which is an equilibrium measurement).[29]

While the formation of a stable skin layer is apparently very important to microgel phase transition curve broadening, the data in Figure 2 suggest that slight modifications to the particle shell do not significantly impact the shape or position of the observed phase transition curve. Only very small differences are observed between the unmodified core−shell particle (sample B) and the BMA-modified core−shell (sample C), while samples C and A (core only) are practically superimposable when plotted as a function of volume change. As described above, the position, magnitude, and breadth of the transition are very similar for all three samples. This is in contrast to published results obtained from macrogels that show strong phase transition temperature perturbations upon introduction of BMA homogeneously throughout the gel monolith.[57] In those experiments, introduction of BMA had a direct impact on the phase transition temperature, as well as on the swelling kinetics. As evidenced by invariance in both the microgel phase transition temperature and in ΔH (Table 2), the thermodynamic insensitivity of our system is also observed when the thickness of the BMA-containing shell is increased (Figure 3a), when low levels of BMA are introduced to both the core and shell (Figure 4), and when the BMA shell concentration is increased (Figure 5a). Together, these results suggest that the solvation energetics of p-NIPAm core−shell microgels are not strongly perturbed by low levels of hydrophobic modification, where the modification can either be homogeneous (e.g., sample D) or isolated to the particle periphery.

This insensitivity is not carried over to the rate of particle collapse, however. As shown in Figure 3c, a <1% concentration of BMA in the microgel shell leads to a >3-fold decrease in the rate of particle collapse versus the unmodified analogue (sample F5). This result is similar to those observed for hydrophobically modified macrogels, where the rate of hydrogel collapse correlates strongly with hydrophobic content.[54,57,58] The origin of the effect in macrogels is attributable to increased skin layer stability. Since the collapse of macrogels is dependent on the ability of water contained inside the gel to diffuse through the skin layer, one would expect that densification of that layer would present a greater barrier to water diffusion. Judging from

(51) Tanaka, T.; Fillmore, D. J.; Sun, S.-T.; Nishio, I.; Swislow, G.; Shah, A. *Phys. Rev. Lett.* **1980**, *45*, 1636−1639.
(52) Guillermo, A.; Addad, J. P. C.; Bazile, J. P.; Duracher, D.; Elaissari, A.; Pichot, C. *J. Polym. Sci., Part B: Polym. Phys.* **2000**, *38*, 889−898.
(53) Matsuo, E. S.; Tanaka, T. *Nature* **1992**, *358*, 482−485.
(54) Yoshida, R.; Sakai, K.; Okano, T.; Sakurai, Y. *J. Biomater. Sci., Polym. Ed.* **1994**, *6*, 585−598.
(55) Suzuki, A.; Yoshikawa, S.; Bai, G. *J. Chem. Phys.* **1999**, *111*, 360−367.
(56) Kaneko, Y.; Sakai, K.; Kikuchi, A.; Aoyagi, T.; Sakurai, Y.; Okano, T. *Proc. Int. Symp. Controlled Release Bioact. Mater.* **1997**, *24th*, 543−544.
(57) Kaneko, Y.; Yoshida, R.; Sakai, K.; Sakurai, Y.; Okano, T. *J. Membr. Sci.* **1995**, *101*, 13−22.
(58) Bae, Y. H.; Okano, T.; Hsu, R.; Kim, S. W. *Makromol. Chem., Rapid Commun.* **1987**, *8*, 481−485.

the strong hydrophobic perturbations shown in Figures 3−5, it is apparent that this effect carries over to microgels, where collapse of the particle exterior presents a thermodynamically stable barrier to water diffusion from the particle core. It is interesting to note that the size-adjusted rate is constant for a given BMA concentration, and is independent of BMA shell thickness (Figure 3c). It is apparent from this result that the rate of microgel collapse is determined solely by the initial formation of the skin layer; increases in the thickness of the hydrophobically modified shell over length scales longer than the skin layer thickness do not further decrease the rate of water diffusion from the particle core. An extreme example of this can be seen by comparing the normalized collapse rates of samples D, F1−4, and G2 (Table 2). Sample D contains a homogeneous distribution of BMA throughout (1% concentration) and does not have a significantly different collapse rate than that of a particle modified with a shell containing roughly the same BMA concentration (F1−4 and G2). However, confining the amount of BMA in sample D to only the microgel shell (sample E) results in a strong perturbation of the collapse kinetics (Figure 4b), as it simply doubles the hydrophobe concentration in the region of initial skin layer formation. These results indicate that it is the location of the modifier that determines the collapse kinetics and not the total mass of BMA in the particle; the *rate determining* skin layer formation occurs only at the outset of particle collapse.

Given this result, the data shown in Figure 5 can be explained in terms of skin layer formation. As the concentration of BMA is increased in the shell, the water diffusion barrier imposed by the skin layer is also increased. This decrease in the rate of water diffusion from the core will in turn cause the particle to reach swelling equilibrium more slowly. The BMA dependence is roughly linear, with a 2.5% BMA concentration resulting in a 3.7-fold decrease in the collapse rate. This seems to be a relatively large modulation of the rate, in light of the fact that the collapse thermodynamics remain unperturbed at these BMA concentrations. In essence, the thermodynamics and kinetics of hydrogel solvation are decoupled in this system. However, close examination of the factors governing equilibrium and nonequilibrium hydrogel swelling can at least qualitatively suggest the origin of this decoupling. Factors affecting the p-NIPAm LCST can usually be traced to changes in the osmotic pressure inside the gel. For example, modulation of the ionic strength or the addition of a linear water-soluble polymer (e.g., PEG) can induce differential changes in the water activity inside and outside the hydrogel and therefore cause osmotic swelling or deswelling effects.[50,59,60] However, the osmotic pressure changes brought about by introducing low concentrations of BMA to the microgel are not very large. BMA is not readily water soluble, and therefore, while it may induce local changes in the hydration environment, these effects should not have a long-range influence on the osmotic pressure. More significantly, the concentration of BMA in these particles is low enough to inhibit aggregation or phase separation into BMA-rich phases; the BMA can be thought of as being isolated in a sea of hydrated p-NIPAm that is not strongly perturbed by its presence. Conversely, deswelling kinetics are more sensitive to changes in the *dynamics* of water diffusion than by small osmotic pressure changes. Since the expulsion of water from the particle is mainly slowed by restricted diffusion through the skin layer, the characteristics of the BMA-modified shell in the *collapsed* state will determine the rate of particle collapse. As the BMA concentration is increased, the hydrophobicity of the skin layer also increases due to a greater degree of hydrophobic aggregation in the polymer. In turn, the water permeability of the more hydrophobic skin layer should be suppressed.

(59) Saunders, B. R.; Vincent, B. *J. Chem. Soc., Faraday Trans.* **1996**, *92*, 3385−3389.

(60) Saunders, B. R.; Crowther, H. M.; Vincent, B. *Macromolecules* **1997**, *30*, 482−487.

Conclusions

Thermoresponsive core−shell microgels with tunable deswellling kinetics have been synthesized by seed and feed precipitation polymerization. Differential scanning calorimetry measurements of particle collapse times show that the addition of small concentrations of a hydrophobic monomer (BMA) localized into the particle shell are sufficient to induce large decreases in the deswelling rate. Conversely, these DSC measurements, along with photon correlation spectroscopy studies, show that the thermodynamics of the particle phase transition are not perturbed by low levels of hydrophobic modification. The collapse time increases monotonically with BMA concentration, while increases in the thickness of the hydrophobically modified shell do not change the deswelling rate. These results suggest that the formation of a thin, stable skin layer at the particle exterior during the early stages of particle collapse is the rate limiting factor in particle deswelling, while the hydrophobicity of the skin layer determines the absolute collapse rate. It is expected that the ability to independently tune the phase transition kinetics and thermodynamics via the core−shell microgel construct will increase the potential utility of these so-called "smart gels" beyond that of homogeneous gel structures.

Acknowledgment. We wish to thank Prof. David Collard and Dr. Rob Krieger for their assistance with, and discussions regarding DSC measurements. L.A.L. gratefully acknowledges financial support from Research Corporation in the form of a Research Innovation Award, from the National Science Foundation for a CAREER Award, and from the Arnold and Mabel Beckman Foundation for a Young Investigator Award.

Supporting Information Available: Figure S1, plot of normalized DSC peak width versus measured BMA content for all particles prepared in this work; Figure S2, plots of mean radius, scattered light intensity, and polydispersity versus temperature for a representative particle (F1); Figures S3, overlaid plots of mean radius and deswelling ratio versus temperature for samples F1−F5; Figure S4, overlaid plots of mean radius versus temperature for samples G0−G5; Figure S5, overlaid plots of scattered light intensity and normalized turbidity versus temperature for samples G0−G5; Figure S6, overlaid plots of scattered light intensity and normalized turbidity versus temperature for samples F1−F5 (PDF). This material is available free of charge via the Internet at http://pubs.acs.org.

JA010609F